Available online at www.sciencedirect.com
ScienceDirect
Surface Science 601 (2007) L29–L33
SURFACE SCIENCE
www.elsevier.com/locate/susc

Surface Science Letters

Prediction of structure-dependent charge transfer rates for a Li atom outside a Si(0 0 1) surface

Keith Niedfeldt [a], Peter Nordlander [b], Emily A. Carter [a,*]

[a] *Department of Mechanical and Aerospace Engineering and Program in Applied and Computational Mathematics, Princeton University, Princeton, NJ 08544-5263, United States*

[b] *Department of Physics and Astronomy, M.S. 61, Rice University, P.O. Box 1892, 6100 South Main Street, Houston, TX 77251-1892, United States*

Received 18 September 2006; accepted for publication 22 December 2006
Available online 4 January 2007

Abstract

We investigate the broadening of the 2s energy level of a Li atom outside a Si(0 0 1) surface using a first principles approach. The covalent nature of the Si surface produces large variations in Li energy level widths as a function of lateral position across the surface. The widths above symmetric Si dimers are predicted to be much larger than above buckled Si dimers, suggesting that charge transfer will occur primarily above symmetric dimers. We discuss the ramifications of our results on the controversy surrounding the relative abundance of the buckled vs. symmetric dimers on the Si surface.

Keywords: Atom–solid interactions, scattering, diffraction; Density functional calculations; Ion–solid interactions, scattering, channeling; Silicon; Low index single crystal surfaces

The fundamental process of charge transfer plays a critical role in many important surface processes such as desorption [1], oxidation [2], and catalysis [3]. It also forms the basis of an experimental technique for probing surface composition and structure, namely low-energy ion scattering (LEIS) [4]. This method typically employs alkali ions, such as Li^+, to scatter off substrates of interest including, e.g., silicon and silicon oxide [5]. The fraction of ions that survive, their angular distributions, and exit velocities are crucial for determining surface structure and composition. Thus, quantifying the ion–surface charge transfer probability from first principles can help interpret such experiments.

The key factor governing the charge transfer probability in such processes is the electron tunneling rate through the potential barrier between the impinging atom (or molecule) and the surface. These electron tunneling rates can be determined from the broadening of atomic (or molecular) energy levels as the gas phase species approaches the surface.

Over the past decade, numerous investigations into charge transfer events in atom–surface scattering off metallic surfaces have produced fairly sophisticated theoretical techniques [6–9] for analyzing charge transfer in gas–surface interactions. These techniques, when coupled to a dynamical theory [10], provide good agreement with experiment [9,10] for scattered ion neutralization fractions on metallic substrates.

In contrast to the situation for metal substrates, charge transfer between atoms and semiconductor surfaces is much less well understood [11,12]. While the chemisorption of atoms on semiconductor surfaces represents one of the most studied classes of systems in surface science [13,14], such calculations have not yet addressed the quantity of relevance for charge transfer, i.e., the broadening of atomic levels as a function of position outside the surface.

For atoms at physisorption distances from metallic surfaces, the interaction between the atom and the surface is dominated by the image potential. The broadening of an

* Corresponding author. Tel.: +1 609 258 5391; fax: +1 609 258 5877.
E-mail address: eac@princeton.edu (E.A. Carter).

0039-6028/$ - see front matter © 2007 Elsevier B.V. All rights reserved.
doi:10.1016/j.susc.2006.12.085

atomic level with decreasing atom–surface separation is caused by the decreased tunneling barrier introduced by image potential effects. The width of atomic resonances therefore can be modeled using simple one-electron model potentials that include the proper image potential parameters [6–8]. Recent work has improved on the simple image model by including model potentials mimicking a realistic band structure of the substrate. These calculations have demonstrated that the band structure of metal surfaces can have a pronounced effect on the broadening of the atomic levels [15].

The situation is more complex on a semiconductor surface. No universal image potential exists;[1] the interactions between the atom and the surface depend critically on both the atomic and the substrate electronic structure, including details of the bonding and hybridization of the electronic states involved.

We presented recently a first principles approach for the calculation of the broadening of atomic levels near surfaces [9,16,17]. In this procedure, the energy level width is obtained from a self-consistent calculation of the electronic structure of the system. We validated our scheme by predicting energy level widths for Li scattering off Al(0 0 1) that were in excellent agreement with experimental data [9]. In this paper, we apply our method to assessing Li charge transfer probabilities above a semiconductor surface of considerable technological importance, namely Si(0 0 1), which is the surface used to create silicon-based computer chips.

The Si(0 0 1) surface structure has long been the subject of controversy [18–28]. The earliest low-energy electron diffraction (LEED) data showed the presence of a 2×1 unit cell [18], which was subsequently interpreted in terms of either buckled [19] or symmetric [20] Si dimers formed from doubly-unsaturated Si atoms on the Si(0 0 1) unreconstructed surface. Much later, the first scanning tunneling microscopy (STM) data showed the presence of both symmetric and buckled dimers [21]. More recent low temperature LEED [26], X-ray photoelectron spectroscopy (XPS) [24], and atomic force microscopy (AFM) [28] experiments have concluded that the lowest energy structure is in fact one in which the dimers are buckled, though the energy difference between the two configurations has been estimated to be very small, by many theoretical methods [27]. Indeed, at finite temperature, the dimers are dynamically buckling, going from buckled to symmetric and back to buckled [14,21,22]. Thus, the surface is at all times a mixture of buckled and symmetric dimers; we will return to this point later.

Unlike the metallic surfaces we investigated earlier, we find that the probability for charge transfer outside a silicon surface exhibits a large lateral corrugation and a strong sensitivity to the instantaneous structure of the surface. The most reactive features of the surface structure are the Si dangling bonds; hence we first investigate the role of the dangling bonds in charge transfer with an incoming adsorbate. We specifically compare the charge transfer probabilities between a symmetric $p(2 \times 1)$ and a buckled $p(2 \times 2)$ Si(0 0 1) surface. We find that charge transfer near symmetric vs. buckled dimers differ both qualitatively and quantitatively. We then discuss the implications of surface dimer interconversion on the overall adsorbate–surface charge transfer rate. The final, quantitative neutralization/ionization rates in an actual Li/Si(0 0 1) scattering event will depend on both these local charge transfer rates we calculate here and the energy of the Li 2s level relative to the positions of the Si dimer HOMO and LUMO levels. These energy shifts were not evaluated here, but could be done in the future. Nevertheless, as we will see, the local charge transfer rates by themselves provide important new insights into the nature of Li/Si(0 0 1) scattering.

We determine charge transfer rate landscapes by post-processing analysis of the self-consistent valence electronic structure of Li above Si(0 0 1) obtained from the periodic DFT program CASTEP_3.2 [29]. Electron exchange and correlation is treated within the spin-polarized local density approximation [30]. Pseudopotentials representing the core electrons and nuclei of Si, H (used to saturate the bottom surface, as described below), and Li are taken from the Trouiller–Martins libraries created by Allan and Teter [31,32]; all valence electrons of each atom are treated explicitly within DFT. The Si(0 0 1) surface is replicated into a Si(0 0 1)-(2×2) supercell containing four atoms per layer. Eight layers of substrate Si atoms and one saturating layer of hydrogen atoms covering the unreconstructed bottom layer of Si are necessary (and hence are used) to properly mimic the semiconductor surface. Periodic images of the surfaces are separated by 38 a.u. of vacuum. Li–Li lateral interactions due to periodic images are negligible for these supercell sizes [9]. Within this supercell, we utilize a k-point spacing of 0.032387 1/a.u. The planewave basis kinetic energy cutoff is chosen to be 400 eV. These numerical parameters are sufficient to converge the Li energy level widths to within a precision of 0.01 eV. We allow a full geometric relaxation of the slab, which resulted in a $p(2 \times 2)$ reconstruction with staggered, buckled dimers. To consider symmetric dimers, the z-coordinates of the top layer Si atoms were constrained to be identical while all other degrees of freedom of the surface were relaxed. The surface was discretized into a 15×15 grid for each distance point

[1] An image-like potential also exists outside a dielectric substrate like Si, but it is not a universal one. The image potential outside a metal is universal in the sense that no matter what the conduction electron density of the metal is, an asymptotic $1/4z$ dependence results (where z is the adsorbate–surface distance). The reason for this universality is that the image potential can be viewed as the interaction of the electron with its exchange-correlation hole, which is constrained to be located inside the surface: a universal phenomenon. However, on a semiconductor, the origin of the image potential is the polarization of the substrate atoms and thus it depends on their polarizability. The resulting "image-like" potential depends inversely on z, but with a proportionality constant that depends on the chemical composition of the surface. The present calculation includes the polarization of the four Si valence electrons within the LDA formalism and thus accounts for some of the dielectric "image-like" potential.

SURFACE SCIENCE LETTERS

above the surface. The Li 2s energy level width was then extracted for each grid point above the surface.

Details of our scheme for extracting energy level widths can be found in [9,12]. We calculate the width of the atomic resonance from the projected density of states (PDOS).

$$\Pi_l(\varepsilon) = 2\pi \sum_m |\langle \phi_m | \phi_l \rangle|^2 \delta(\varepsilon - \varepsilon_m) \quad (1)$$

In Eq. (1), the PDOS $\Pi_l(\varepsilon)$ is a function of the energy ε and the state l onto which we project. This function is evaluated by calculating the overlap of m interacting adsorbate + surface Kohn–Sham orbitals ϕ_m with the valence orbital ϕ_l of an adsorbate placed at infinity. The Dirac delta function $\delta(\varepsilon - \varepsilon_m)$, where ε_m is the energy of interacting orbital m, is then initially broadened using a small parameter. The PDOS obtained in this way is a Lorentzian from which a width may be extracted using a deconvolution scheme that eliminates the initial broadening parameter.

Fig. 1 displays contour plots of the width of the Li 2s level as a function of lateral position around buckled dimers (a) and symmetric dimers (b) on the Si(001) surface. In Fig. 1b we see that the level widths are almost three times larger above the pseudo-π bonds (comprised of the symmetric combination of the two silicon dangling bonds) than above the troughs between the dimer rows (located at the top and bottom of the figure). Additionally, we see that the 2s level widths are significantly larger above symmetric dimer configurations than above the dangling bonds of the buckled dimers.

Although the calculated Li 2s energy level widths depend on lateral position, the distance to the surface also strongly affects the widths. In Fig. 2, we see that Li 2s energy level widths decrease as a function of distance from the surface, as expected. However, the energy level widths do not decay exponentially, as in the cases for Li above metal surfaces. Oscillations in the widths as a function of distance correspond to local surface effects such as Li interactions with the dangling bond comprising the surface LUMO, as discussed below. Moreover, we see that the fall-off in the widths is much slower for the symmetric dimer, suggesting that at long range the charge transfer may be controlled by the instantaneous population of symmetric dimers.

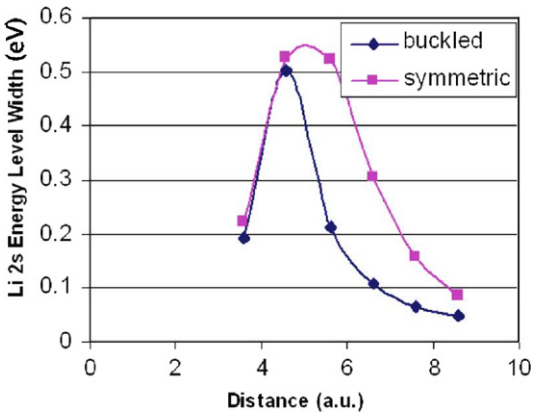

Fig. 2. Li 2s energy level widths (eV) as a function of distance to the Si(001) surface above the Si dangling bond site (directly above the down dimer atom in the buckled dimer surface). The Li–Si(001) surface distance is defined as in Fig. 1.

Fig. 3 displays contour plots of the broadening of the Li 2s level in a plane perpendicular to the surface. The lateral position along the surface supercell is shown on the horizontal axis and the distance from the surface is shown on the vertical axis. The level width outside the symmetric dimer Si(001)-(2 × 1) surface (Fig. 3b) is quite different than for the buckled dimer surface (Fig. 3a). The decrease of the width with increasing Li–Si separation is much

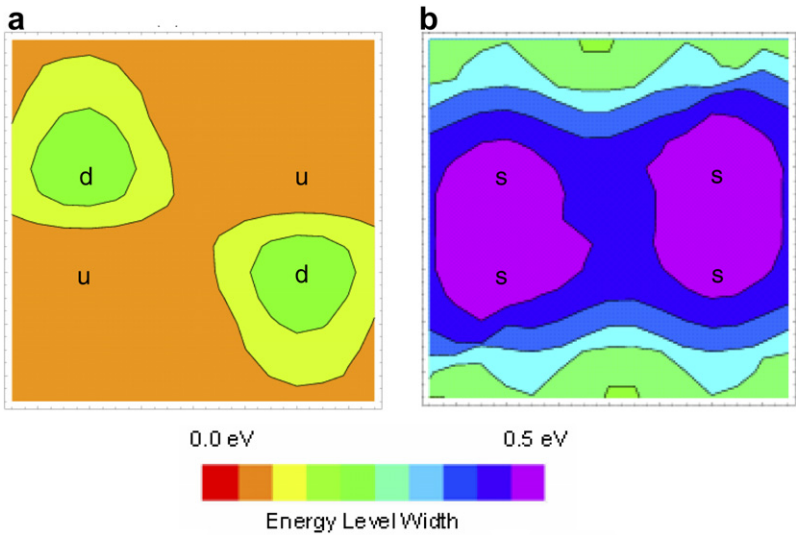

Fig. 1. Two-dimensional Li 2s energy level width landscape for Li 5.6 a.u. above the Si(001) surface. The distance of 5.6 a.u. is defined relative to the average of the surface Si dimer atoms' z-coordinates. (a) The width profile for Li above buckled Si dimers (u denotes position of up buckled dimer atom, d of down dimer atom). (b) The width profile above symmetric Si dimers (s are positions of symmetric dimer atoms 5.6 a.u. below this 2D slice). The width landscape is not perfectly symmetric due to imperfect sampling of the landscape.

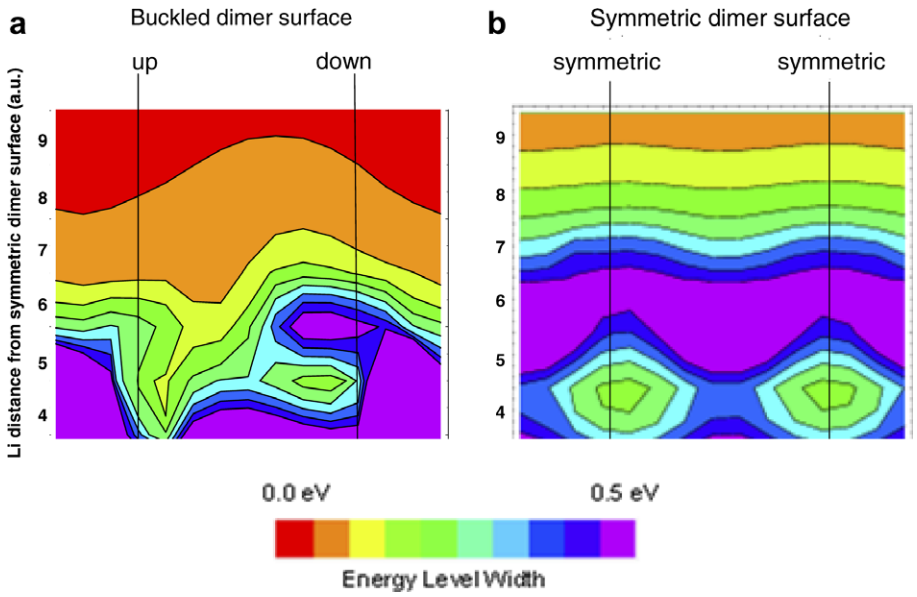

Fig. 3. 2D vertical Li 2s energy level width landscape sliced through a Si dimer on the Si(0 0 1)-(2 × 1) surface. The horizontal axis represents the lateral surface position and the vertical axis represents the distance from the surface. Lines correspond to the positions of the Si dimer atoms, with the up dimer atom and the down dimer atom in (a), and the symmetric dimer atoms in (b).

slower for the symmetric dimers, as already noted above. It is also clear from Fig. 3 that the oscillations in widths seen in Fig. 1 are due to localized interactions with either the down dimer atom of the buckled dimer or the symmetric dimer atoms. Fig. 3 shows that both dimer structures produce a strong lateral corrugation in the widths at all distances.

The interconversion of buckled and symmetric Si dimers on the surface itself presents an additional complication. As we have shown, the adsorbate resonance widths are vastly different depending on whether the adsorbate interacts with buckled or symmetric Si dimers. As schematically depicted in Fig. 4b, the buckled dimer is well known to have a polar electronic structure, namely intra-dimer electron transfer occurs from the down dimer atom to the up dimer atom, rendering the up dimer atom somewhat negatively charged and consequently the down dimer atom is somewhat positively charged [20,23,24,33,34]. As a result, in the buckled state, the lowest unoccupied molecular orbital (LUMO) is localized on the down dimer atom, while the highest occupied molecular orbital (HOMO) is localized on the up dimer atom. Thus, ionization of a neutral Li atom is most likely to involve the LUMO at the down Si dimer atom, while neutralization of a Li ion would be dominated by interaction with the HOMO at the up Si dimer atom. This is entirely consistent with Figs. 1 and 3, in which we see that the largest neutral Li 2s level widths for the buckled dimer occur over the down dimer atom, the position of the LUMO. By contrast, charge transfer from a neutral Li atom to the symmetric state is expected to involve tunneling into the pseudo-π^* (antibonding) LUMO of the Si–Si dimer bond, while the back electron transfer to an ionized Li will involve tunneling from the pseudo-π (bonding) HOMO of the Si–Si dimer bond (see Fig. 4a). Again, this

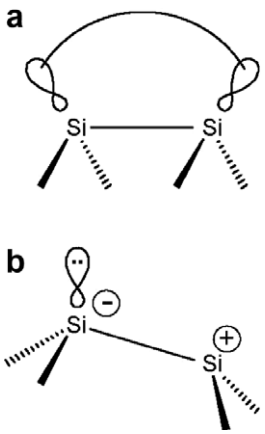

Fig. 4. Schematic of the polarization and highest occupied molecular orbitals (HOMOs) of the (a) symmetric and (b) buckled dimers on the Si(0 0 1)-(2 × 1) surface. The symmetric dimer is nonpolar with a π-like HOMO where the Si dangling bond electrons are spin-coupled (as depicted by the solid curve) into a singlet state. The symmetric dimer lowest unoccupied molecular orbital (LUMO) is π^*-like, with a node between the dangling bonds but with the same nonpolar character. The buckled dimer exhibits charge transfer with the HOMO fully localized on the up Si atom (negatively charged) and the LUMO fully localized on the down Si atom (positively charged).

is entirely consistent with Figs. 1 and 3, wherein we see a symmetric distribution of widths above the symmetric dimer atoms. Thus, the charge transfer probability landscape from neutral vs. ionic gas phase species are expected to be very different along the dimer bond for a buckled dimer, while either neutral or ionic Li will exhibit similar charge transfer to/from a symmetric dimer, since the HOMO and LUMO are both localized in the same place along the dimer bond for a symmetric dimer. Of course, the final probability of charge transfer will also depend on the posi-

tion of the Li 2s level relative to the HOMO and LUMO Si dimer levels.

As mentioned above, controversy exists regarding the relative abundance of symmetric vs. buckled dimers on the Si(0 0 1)-(2 × 1) surface [18–28]. This controversy is quite relevant to predicting overall neutralization fractions for scattered Li, since the overall neutralization probability will depend strongly on the proportion of Li atoms that interact with the Si surface in the symmetric vs. buckled dimer configuration. STM measurements suggest that the ratio of buckled to symmetric dimers is increased as the temperature is lowered [25]. Our results suggest that symmetric dimers may dominate the neutralization process, especially at large adsorbate–surface distances. Based on the LEED conclusions mentioned earlier [26], we would predict that LEIS will yield higher neutralization fractions for the same Si(0 0 1) substrate as it is heated up from 120 K, since the instantaneous population of symmetric Si dimers will increase with temperature.

To summarize, a highly corrugated charge transfer probability landscape is predicted for Li atom above Si(1 0 0), due to surface structural features (i.e., Si dimers) that control local electron tunneling rates. Charge transfer from Li above a buckled dimer is greatest above its down atom, consistent with its electronic structure (positively-charged down atom). The symmetric dimer yields the largest Li widths overall, consistent with its semi-metallic electronic structure (π-bonding). These larger and longer-range widths suggest that the symmetric state may be largely responsible for the neutralization of scattered Li ions in LEIS. Given that the population of symmetric vs. buckled dimers is thought to be temperature dependent, we predict that changing the surface temperature may strongly influence the neutralization fractions measured in LEIS. Calculations of the Li 2s energy level shifts in the future will provide a complete evaluation of ionization/neutralization rates to validate these ideas further.

Acknowledgements

E.A.C. is grateful to the National Science Foundation for support of this research. P.N. is grateful to the Robert A. Welch Foundation (Grant No. C-1222). K.N. thanks Dr. Robin Hayes for useful discussions. We thank Accelrys, Inc. for providing the CASTEP software and thank Dr. Patrick Huang for graphical assistance.

References

[1] H. Petek, H. Nagano, M.J. Weida, S. Ogawa, Journal of Physical Chemistry B 105 (2001) 6767.
[2] N. Cabrera, N.F. Mott, Reports on Progress in Physics 12 (1948) 163.
[3] B. Hammer, J.K. Norskov, Advances in Catalysis, vol. 45, Academic Press Inc, San Diego, 2000, p. 71.
[4] W. Heiland, E. Taglauer, Methods of Experimental Physics, vol. 22, Academic, Orlando, FL, 1985.
[5] Y. Yang, J.A. Yarmoff, Surface Science 573 (2004) 335.
[6] P. Nordlander, J.C. Tully, Physical Review Letters 61 (1988) 990.
[7] D. Teillet-Billy, J.P. Gauyacq, Surface Science 239 (1990) 343.
[8] P. Kurpick, U. Thumm, Physical Review A 58 (1998) 2174.
[9] K. Niedfeldt, E.A. Carter, P. Nordlander, Journal of Chemical Physics 121 (2004) 3751.
[10] H.X. Shao, D.C. Langreth, P. Nordlander, Physical Review B 49 (1994) 13929.
[11] E.A. Garcia, C.G. Pascual, P.G. Bolcatto, M.C.G. Passeggi, E.C. Goldberg, Surface Science 600 (2006) 2195.
[12] M. Taylor, P. Nordlander, Physical Review B 64 (2001) 115422.
[13] H.N. Waltenburg, J.T. Yates, Chemical Reviews 95 (1995) 1589.
[14] R.J. Hamers, Y.J. Wang, Chemical Reviews 96 (1996) 1261.
[15] A.G. Borisov, A.K. Kazansky, J.P. Gauyacq, Surface Science 430 (1999) 165.
[16] K. Niedfeldt, P. Nordlander, E.A. Carter, Physical Review B 74 (2006) 115109.
[17] K. Niedfeldt, E.A. Carter, P. Nordlander, Surface Science 600 (2006) L291.
[18] R.E. Schlier, H.E. Farnsworth, Journal of Chemical Physics 30 (1959) 917.
[19] D.E. Eastman, Journal of Vacuum Science and Technology 17 (1980) 492.
[20] A. Redondo, W.A. Goddard III., Journal of Vacuum Science and Technology 21 (1982) 344.
[21] R.J. Hamers, R.M. Tromp, J.E. Demuth, Physical Review B 34 (1986) 5343.
[22] P.C. Weakliem, G.W. Smith, E.A. Carter, Surface Science 232 (1990) L219.
[23] G.K. Wertheim, D.M. Riffe, J.E. Rowe, P.H. Citrin, Physical Review Letters 67 (1991) 120.
[24] E. Landemark, C.J. Karlsson, Y.C. Chao, R.I.G. Uhrberg, Physical Review Letters 69 (1992) 1588.
[25] R.A. Wolkow, Physical Review Letters 68 (1992) 2636.
[26] M. Kubota, Y. Murata, Physical Review B 49 (1994) 4810.
[27] Y.S. Jung, Y.H. Shao, M.S. Gordon, D.J. Doren, M. Head-Gordon, Journal of Chemical Physics 119 (2003) 10917.
[28] Y.J. Li, H. Nomura, N. Ozaki, Y. Naitoh, M. Kageshima, Y. Sugawara, C. Hobbs, L. Kantorovich, Physical Review Letters 96 (2006) 106104.
[29] M.D. Segall, P.J.D. Lindan, M.J. Probert, C.J. Pickard, P.J. Hasnip, S.J. Clark, M.C. Payne, Journal of Physics—Condensed Matter 14 (2002) 2717.
[30] J.P. Perdew, A. Zunger, Physical Review B 23 (1981) 5048.
[31] M.C. Payne, M.P. Teter, D.C. Allan, T.A. Arias, J.D. Joannopoulos, Reviews of Modern Physics 64 (1992) 1045.
[32] X. Gonze, G.M. Rignanese, M. Verstraete, J.M. Beuken, Y. Pouillon, R. Caracas, F. Jollet, M. Torrent, G. Zerah, M. Mikami, P. Ghosez, M. Veithen, J.Y. Raty, V. Olevanov, F. Bruneval, L. Reining, R. Godby, G. Onida, D.R. Hamann, D.C. Allan, Zeitschrift Fur Kristallographie 220 (2005) 558.
[33] D.J. Chadi, Physical Review Letters 43 (1979) 43.
[34] R.J. Hamers, R.M. Tromp, J.E. Demuth, Surface Science 181 (1987) 346.